Compact 1.7 K Cryocooler for Superconducting Nanowire Single-Photon Detectors

V. Kotsubo, J.N. Ullom, and S.W. Nam

National Institute of Standards and Technology
Boulder, CO 80305, USA

ABSTRACT

State-of-the-art superconductor-based cryogenic detector systems are being installed at numerous research facilities worldwide and are achieving world-record sensitivities in a variety of applications. Implementation has been greatly facilitated by closed-cycle refrigeration. However, in many cases, cooling capacities of the refrigerators exceed requirements, at times by orders of magnitude, resulting in excessively large and cumbersome systems. The availability of more compact and lower power consumption systems should greatly facilitate further user acceptance. Toward this end, we are developing a compact 1.7 K closed-cycle pulse tube/Joule-Thomson hybrid cryocooler for superconducting nanowire single-photon detectors. A laboratory prototype consisting of the pulse tube cooler and the Joule-Thomson coldhead has demonstrated over 1.4 mW of cooling at 1.7 K. The Joule-Thomson compressor is under development and remains the single largest risk item in terms of reliability. The system, designed for low manufacturing costs, is projected to consume on the order of 250 W total power, including power for cooling fans, thermometry, and detector electronics, and to be mountable within a standard equipment rack.

INTRODUCTION

Applications for superconductor-based sensors and electronics have been steadily increasing over the past several years in diverse areas such as astrophysics/cosmology,[1] X-ray spectroscopy,[2] gamma-ray spectroscopy,[2] quantum information,[3] and photon science.[3] These systems operate at temperatures ranging from above 4 K to lower than 50 mK. Although these systems are developed by scientists with low-temperature expertise, end users typically have minimal cryogenic experience, and therefore acceptance has been greatly facilitated by push-button, closed-cycle cryocoolers. The majority of these systems depend on precooling with commercial Gifford-McMahon or valved pulse tube coolers, which were originally developed for applications requiring relatively large cooling capacities such as shield cooling in magnetic resonance imagers or cryopumping. As a result, for many, if not most of these systems, the size and power consumption of the system are orders of magnitude larger than necessary. For example, many transition edge sensor (TES) systems are cooled using adiabatic demagnetization refrigerators (ADRs) with cooling capacities of hundreds of nanowatts at temperatures below 100 mK. At the 4 K reject temperature for the ADR, the heat rejected is on the order of a milliwatt, yet precoolers with capacities on the order of a watt with a power draw of several kilowatts are used.

Cryocoolers 20, edited by S.D. Miller, R.G. Ross, Jr. and J.R. Raab

While there are advantages for using excessively large coolers such as rapid cooldown times and flexibility in cryostat design, future widescale applications of these types of systems will be greatly enhanced by reducing their size and power. Such applications include secure quantum encrypted communication links[3] that utilize superconducting nanowire single-photon detectors (SNSPD), and superconducting transition-edge sensor microcalorimeters for electron microscope microanalysis.[2]

Based on these considerations, we initiated the development of a compact cooler for an SNSPD detector system that will result in a form factor and low power draw of a standard rack- mountable electronics instrument. The cooler is a pulse tube/Joule-Thomson (PT/JT) hybrid, with the JT stage achieving 1.4 mW of cooling at 1.7 K, and the three-stage pulse tube providing cooling at 80 K, 25 K, and 10 K. To date we have successfully developed the pulse tube cooler and JT coldhead, whereas the JT compressor and associated gas decontamination is still under development.

We have previously published results on an early version of this cooler.[4] In this paper we present further details, plus improvements, including a modification of the pulse tube 10 K stage regenerator that increased the cooling capacity at 10 K by 35 % and reduced the minimum temperature from 7.8 K to 6.4 K; and a modification of the JT stage, which dropped the minimum temperature from 2.2 K to 1.7 K.

CRYOCOOLER DESCRIPTION

Design Goals

As discussed in a previous publication[4] the target application is a four-channel tungsten-silicide (WSi) SNSPD.[5] Estimated cooling loads on each of the cooler stages are presented in Table 1 along with the design goals. The cooling load on the JT stage arises primarily from low thermal conductance bias/readout coaxial cables, since SNSPD's dissipate negligible power and photons are coupled in through optical fiber. Our targeted cooling capacities included design margin on each stage. The 80 K stage radiation load estimate has considerable uncertainty due to unknown ambient temperature since the cryocooler will be enclosed in an equipment rack-mounted box, and because of the uncertain surface emissivity of the radiation shield.

The WSi SNSPD detectors require cooling to 1.25 K for maximum quantum efficiency, but this temperature is difficult to achieve with a ^{4}He JT refrigerator that utilizes a low power, compact compressor. A ^{3}He JT would reach this temperature and will be used for future units, but to facilitate development, we used ^{4}He and targeted 2.0 K since the identical vapor pressure if ^{3}He is used would result in 1.25 K. Operation at temperatures up to 2.5 K is acceptable if maximum quantum efficiency is not required.

The 10 K for the precooling temperature for the JT stage is a lower temperature than the thermodynamic optimum for this hybrid, but we opted for as low as reasonable precooling temperatures to reduce the high-pressure requirement for the JT loop, which in turn reduces stress on the JT compressor. We chose this approach because the JT compressor is the largest risk to reliability. Final test results shown below show that the actual operating temperature of this stage was below 7.7 K

Table 1. Estimated heat loads and design goals for a four channel SNSPD detector cooler.

Stage	Radiation (mW)	JT Precooling (mW)	Conduction (mW)	Total (mW)	Design Target (mW)
80 K	1000-2350	400	150	1550-2900	3000
25 K	5-12	28	7	40-47	100
10 K	0.2	2	1	3.2	5
2.0K	0	N/A	0.28	0.28	0.5

.

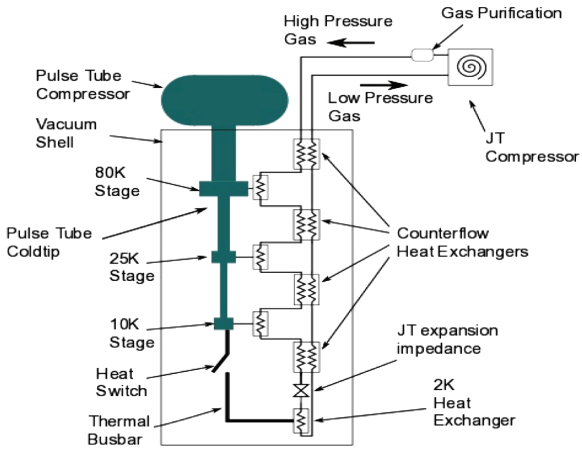

Figure 1. Operational schematic of the cryocooler.

Cooler Description

The cooler is shown schematically in Figure 1. The pulse tube is a three-stage, cooled inertance tube[6] configuration driven by a commercial resonant piston compressor at 35 Hz. Each stage is a U-tube configuration, resulting in an easy-to-integrate coldhead. Because the objective of the project is a producible, low cost cooler, the mechanical design sacrificed performance to reduce costs. The most impactful tradeoff was the use of standard sized stainless-steel tubing for the regenerator and pulse tube walls, rather than machined titanium, which is commonly used in aerospace coolers. Replacing the stainless-steel tubes with titanium tubes would result in 1.8 W, 0.07 W, and 0.001 W of additional cooling on the 80 K, 25 K, and 10 K stages, respectively.

The upper two-stage inertance tubes were dual diameters, whereas the third stage used only a single diameter because modeling indicated minimal improvement in performance with dual diameters. Regenerators used standard materials; the first stage used die-punched stainless-steel screens, with #150 mesh, 66 um wire diameter in the warm side and #400 mesh, 25.4 um wire diameter in the cold side. The second stage used #400 mesh, 25.4 um wire diameter stainless steel screens in the warm side and #400 mesh, 25.4 um wire diameter phosphor bronzes screens, flattened to produce 0.55 porosity, in the cold side. The third stage used high heat capacity microspheres. In the previous work reported in Ref. 4, 100 um diameter 50-50 erbium-praseodymium (ErPr) alloy spheres[7] were used. We have since replaced the lower half of the regenerator with 100 um diameter erbium-nickel (ErNi) spheres to improve cooling capacity below 10 K, and comparative tests results are presented below.

A critical mechanical design objective is geometries that minimize the effects of secondary flows within the pulse tube and regenerator, because these flows can seriously degrade performance. Most well-known are turbulence/convection in the pulse tube and streaming in regenerators.[8] Somewhat less appreciated are secondary flows in the displacer gap in Stirling coolers. A net circulation can flow through the displacer gap and return through the regenerator partially unregenerated and cause cooling loss unless there is sufficient lateral thermal conduction. Alternatively, because the displacer gap is dynamic, the local gap dimensions can vary during the operating cycle, causing local oscillating flows to not exactly reverse motion, again leading to unregenerated flow and cooling loss.

While it is well documented that, in large diameter regenerators, net circulation can lead to significant degradation in coolers,[8] we were concerned that even in small diameter regenerators, some level of circulation can exist, causing measurable cooling loss. In multi-stage coolers, circulation can be generated in the regenerators near the junctions between stages, where the phasing of the flows between the upper stage regenerator, lower stage regenerator, and buffer tube will necessarily lead to circulation in the regenerators if the upper and lower stage regenerators are in-line with each

other because flows entering the regenerator can come from either the adjacent regenerator or the flow channel from the buffer tube. To mitigate this, we located the second stage regenerator such that the warm entrance was in the connecting channel between the first stage regenerator and first stage pulse tube rather than directly in-line with the first stage regenerator. Thus, the flow entering the cold end of the first stage regenerator always came from the channel. This arrangement was not possible for the junction between the second stage and third stage regenerators because the second stage regenerator packing access was through an attachment flange for the third stage regenerator, which was directly in line with the second stage regenerator. However, the small diameters of the second and third stages likely mitigated any effects of circulation. We have not validated whether this design feature improves cooling, but because the cooler performs as predicted by the model, it does not appear that there are any detrimental effects.

For the JT system, the very low cooling capacity requirement allowed a design driven by ease of fabrication rather than by thermodynamics. The stage nominally operates between a high pressure of 200 kPa and a low pressure of 3.2 kPa, with a flow rate of 0.6 mg/s. The thermodynamic power required to recompress the gas is only a few watts, which is such a small fraction of the total power budget that a highly thermodynamically efficient design is not required.

All four JT counterflow heat exchangers were simple tube-in-tube designs, with high-pressure gas flowing in the narrow annular space between the two tubes and the low-pressure gas flowing through the inner tube. This configuration simplifies fabrication, plus has a large internal surface area on the high-pressure return side to allow condensable contaminants to freeze out without plugging the flow passage. The expansion impedance was a 2 m long, 50 μm inner-diameter stainless steel capillary.

At the cold ends of the warmer three counterflow heat exchangers, a small heat exchanger consisting of fine mesh copper screen diffusion bonded to a copper body was used to heat sink the incoming gas to the pulse tube. The 1.7 K coldstage also had a small copper screen mesh heat exchanger for thermal contact to the load.

To mitigate particulate contamination, sintered stainless steel particulate filters were inserted in the high-pressure line prior to entering the cryostat, at the end of the heat exchanger at 80 K and just upstream of the JT expansion impedance. In addition, a small capsule of activated charcoal was placed in the high-pressure stream on the 80 K stage to adsorb any condensable contaminants.

To expedite cooldown of the JT coldstage from room temperature, a heat switch consisting of a small bar that clamped down on a small copper tab attached to the JT coldhead was used. The clamp was heat-sunk to the pulse tube 10 K stage and was actuated by pulling on a fine stainless-steel wire attached to the bar. The far end of the wire was fed through a bellows feedthrough through the room temperature vacuum flange to allow actuation of the heat switch.

In the original system,[4] both the inlet and outlet of the JT expansion capillary were housed in the same copper block and therefore at the same temperature. In this version, we separated the warm and cold ends of the capillary, and the result, presented below, was a lower base temperature of 1.7 K in comparison to the 2.2 K base temperature previously reported.

The JT compressor under development is a scroll compressor, selected because of the ability to achieve low suction pressures, compact size, and low per-unit cost.

MODELING RESULTS

Pulse Tube

The pulse tube was modeled using a widely used commercial Stirling and pulse tube software design package.[9] We relied heavily on the built-in numerical optimizing algorithm to design the cooler so, at least on paper, this is a highly efficient design. In this section we present modeling results, and although most of these model outputs are not easily measurable, we present them as an illustration of cooler behavior.

Table 2 presents top-level parameters of the pulse tube: frequency, charge pressure, oscillatory pressure amplitude P_1, compressor power, and cooling powers. The cooling powers identically match the design goals because those were set as constraints in the optimizer. The compressor power was the result of the optimization process that required its minimization.

Table 2. Modeled Top Level Pulse Tube Parameters

Frequency (Hz)	35
Charge Pressure (MPa)	1.5
Pressure Amplitude P_1 (MPa)	0.13
Compressor Power (W)	148
$\dot{Q}$ 1st stage @ 80 K (W)	3.00
$\dot{Q}$ 2nd stage @ 25 K (W)	0.10
$\dot{Q}$ 3rd stage @ 10 K (W)	5.0×10−3

Table 3. Modeled Compressor Loss

Total Compressor Power (W)	148
Delivered Acoustic Power (W)	117.5
Ohmic Loss (W)	17
Friction/Eddy Current Damping (W)	8.5
Compression Space Heat Transfer (W)	2.5
Seal Blowby (W)	2.5

The charge pressure of 1.5 MPa was driven by the limited regenerator heat capacity below 10 K, and this lower pressure sacrificed thermodynamic efficiency at the higher stages for increased thermodynamic efficiency at the lowest stage.

Table 3 lists the modeled losses for the pulse tube compressor, where the analysis used compressor parameters provided by the vendor. The ohmic loss is particularly small for this type of cooler because the compressor was significantly larger than necessary, with the capability of 600 W of input power.

Table 4 shows regenerator energetics. $\dot{E}_2$ is the second-order acoustic power, defined within the thermoacoustic framework[10] as:

$$\dot{E}_2 = \langle P_1 U_1 \rangle \tag{1}$$

where P_1 is the first order pressure amplitude and U_1 is the first order volume flow rate defined as:

$$U_1 = A_c v \tag{2}$$

where A_c is the cross-sectional flow area, v is the local spatial averaged velocity, and the brackets denote time averaging. The modeling includes higher harmonics, but the acoustic power associated with the fourth-order term is negligible so only the second-order acoustic power is presented. $\dot{H}_{cold}$, $\dot{Q}_{screen}$ and $\dot{Q}_{tube}$ are the enthalpy, screen conduction, and tube wall conduction losses. The enthalpy and screen conduction loss were taken at the cold end of the regenerator because the model couples these two losses internally within the regenerator. As a figure-of-merit, we define the acoustic power loss ratio as:

$$\varepsilon_{\dot{W}_2} = \left(\frac{\dot{E}_{2,cold}}{\dot{E}_{2,hot}}\right) \Bigg/ \left(\frac{\dot{E}_{2,cold,ideal}}{\dot{E}_{2,hot,ideal}}\right) = \left(\frac{\dot{E}_{2,cold}}{\dot{E}_{2,hot}}\right) \times \left(\frac{T_{hot}}{T_{cold}}\right) \tag{3}$$

where, for an ideal lossless regenerator using an ideal gas, the ratio of the acoustic powers at the ends of the regenerator scale as the ratio of the temperatures. The subscripts *hot* and *cold* refer the hot and cold ends of the regenerator. The acoustic power loss ratio therefore indicates the remaining fraction of the ideal acoustic power not consumed by irreversibilities such as viscous loss, within the regenerator.

The second figure-of-merit is the ratio:

$$\varepsilon_{\dot{H}} = \frac{\dot{E}_{2,cold} - \dot{H}_{cold}}{\dot{E}_{2,cold}} \tag{4}$$

which represents the fraction of the gross cooling power remaining after subtracting the enthalpy flow loss. The results of Table 4 indicate that acoustic power loss and enthalpy loss dominate, with

Table 4. Modeled Regenerator Energetics.

	$\dot{E}_{2,hot}$ (W)	$\dot{E}_{2,cold}$ (W)	$\dot{H}_{cold}$ (W)	$\dot{Q}_{screen}$ (W)	$\dot{Q}_{tube}$ (W)	ε_{W_1}	$\varepsilon_{\dot{H}}$
1st stage	111.6	19.0	5.80	0.53	1.32	0.66	0.69
2nd stage	3.46	0.97	0.50	0.026	0.048	0.90	0.48
3rd stage	0.086	0.031	0.01	8.0×10−5	0.0013	0.90	0.68

sizable acoustic power loss occurring in the first stage regenerator, while enthalpy losses occur in all three regenerators but is the largest in the second stage. Part of the reason for high second stage enthalpy loss is that it is operating near its minimum temperature of about 21 K. The high acoustic power efficiencies of the second and third stages in comparison to the first stage suggests that, by using commercially available screen meshes, the hydraulic diameters are larger than optimum, resulting in higher enthalpy losses but lower acoustic losses.

Table 5 shows the energetics of the thermal buffer tubes. The efficiency is:

$$\varepsilon_{TBT} = \frac{\dot{H}_{cold}}{\dot{E}_{2,cold}} \tag{5}$$

In the model, the enthalpy loss and tube wall thermal conduction loss are coupled so that the losses shift between the two along the length of the tube, so the enthalpy and tube conduction are taken at the cold end of the tube. The efficiencies are reasonably high, with one of the contributing factors being the low fluid displacement amplitudes, in the range of 10 % of the total length.

Joule-Thomson Modeling

Because of the very low flow rates and low thermodynamic compression power, the JT loop did not require a high degree of optimization, so counterflow heat exchangers were designed for ease of fabrication. They were modeled using a simple NTU analysis[11] using temperature-averaged fluid properties, along with a separate calculation of thermal conduction down the heat exchanger tubes. There was considerable leeway in the design, allowing heat exchanger lengths to vary by a factor of two without significantly affecting performance. The main consideration was minimizing the demand on the JT compressor, so the system was designed for the lowest reasonable high-side pressure to minimize stresses on bearings and backleakage through seals. Final flow and pressure requirements for the compressor were determined from test data.

TEST RESULTS

Pulse Tube Results

Prior to integration with the JT stage, the pulse tube was tested as a stand-alone unit. It was installed in a laboratory test dewar, with the warm-end temperature controlled to 310 K using temperature-regulated circulating water to simulate the anticipated higher temperature environment when the unit is installed within a fan-cooled equipment rack. The test dewar was not temperature controlled; its temperature varied considerably because the laboratory temperature was unregulated. As a result, there was significant run-to-run variability in the radiation load on the 80 K stage. The PT compressor and first-stage inertance tube were also not temperature regulated, which also led to some first-stage performance variability.

Modeling of the inertance tubes is generally not expected to be accurate because of turbulence, sensitivity to tube diameter, and uncertainty in the heat sink temperature, so an initial tuning of the inertance tube was required. Because inertance tubes for small capacity coolers are effectively low-*Q* quarter-wavelength acoustic resonators, the tubes were tuned by sweeping the drive frequency of the compressor and searching for the frequency of the maximum cooling capacity of each stage. The lengths of the inertance tubes where trimmed or extended by the ratio of this frequency to the resonant frequency of the compressor. The tubes were designed with as low a Q as possible to reduce sensitivity to length and temperature.

Upon completion of this tuning, the first characterization test was to simply measure the

Table 5. Energetics of the thermal buffer tube.

	$\dot{E}_{2,\mathrm{cold}}$ (W)	$\dot{H}_{\mathrm{cold}}$ (W)	ε_{TBT}	$\dot{Q}_{\mathrm{tube}}$ (W)
1st stage	14.2	10.4	0.73	0.42
2nd stage	0.82	0.68	0.83	0.043
3rd stage	0.021	0.017	0.81	7.4×10−4

cooling powers for each stage at their nominal design temperatures of 80 K, 25 K, and 10 K with 150 W compressor power. The results are tabulated in Table ww, with a drive frequency of 35 Hz and charge pressure of 1.5 MPa. The 10 K stage regenerator for this test consisted of all ErPr spheres. The measured loads are in addition to an unknown amount of radiation loading so the actual cooling capacity is somewhat higher on the 80 K and 25 K stages than shown in the table. Reasonable estimates of the radiation load suggest that the cooling power of the 80 K stage is in excess of the design point goal of 3.0 W.

Figures 2a and 2b show the cooling capacities of the 80 K stage and 25 K stage as a function of temperature. Each load curve was taken while holding the other two stages at constant temperature. These plots illustrate that the 80 K stage handles loads on the order of watts, while the 25 K stage handles loads on the order of tenths of watts.

Figure 3 show load curves for the 10 K stage and compares the performance of the all ErPr regenerator and the regenerator with ErPr in the warm half and ErNi in the cold half, with data for ErPr/ErNi regenerator combination shown at three different charge pressures. In all cases the ErPr/ErNi regenerator outperforms the all-ErPr regenerator, except at temperature above 10 K with 1.25 MPa charge pressure for the ErPr/ErNi regenerator. The ErPr/ErNi combination also consistently reached a minimum temperature in the 6.3 K to 6.5 K range while the minimum temperature of the all ErPr regenerator reached a minimum temperature slightly below 8 K. These lower temperatures were expected because of the lower heat capacity of ErPr compared to ErNi at lower temperatures. These data were taken with no applied load to the upper two stages such that the upper stages ran colder than the data in Table 6, which resulted in higher 10 K cooling capacity.

Joule Thomson Results

Because the JT compressor is still under development, final tests on the integrated JT-pulse tube coldhead was conducted open loop using a regulated compressed gas storage bottle as a supply and a vacuum pump vented to atmosphere on the return. The low side pressure was controlled by adjusting a valve in front of the vacuum pump.

Figure 4 shows load curves at high side pressures of 0.2 MPa, 0.15 MPa, 0.125 MPa, and 0.1 MPa. A maximum of 1.4 mW was produced at the minimum temperature of about 1.7 K. The cooling capacity increase at lower temperatures is from increased mass flow through the capillary from higher gas density. Operating at 0.1 MPa does not provide sufficient cooling to cool down the JT stage from the initial temperature of around 7 K.

Table 6. Simultaneously measured cooling capacities at all three stages with 150 W compressor power.

Stage	Temperature (K)	Capacity (W)
1	80	2.77
2	25	0.080
3	10	5.0×10−3

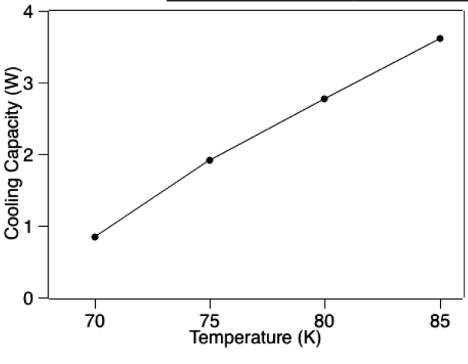

Figure 2a. Load curve for the 80 K stage

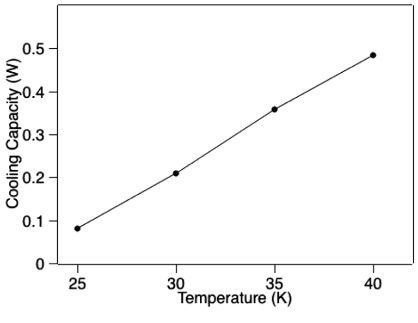

Figure 2b. Load curve for the 25 K stage

In the previous publication we reported instability at the lowest temperatures.[4] In the present setup, the instability occurs only when the temperature of the upstream side of the capillary drops below the liquefaction temperature corresponding to high side pressure. We attribute this to liquid in the low-pressure pumping line reaching the cold end of the JT counterflow heat exchanger, which then liquefies the fluid entering the capillary. Although we do not specifically know why this causes the instability, if we temperature-regulate the coldstage slightly above the minimum temperature, no liquid accumulates, which stabilizes the cold stage temperature.

The return pressure in these tests was as low as 650 Pa. The return pressure does not affect the load curves except that lower temperatures are reached with lower return pressures as expected from the saturation curve.

During these tests, the load on the pulse tube from circulating ^{4}He would cause the third stage temperature to rise slightly. However, in all situations the temperature remained below 7.7 K, indicating that Nb-Ti wire can be used for electrical leads between the 10 K stage and the JT stage.

Cooldown Time

The system cooled to base temperature within 24 h. The 80 K pulse tube stage reached close to its minimum temperature in about 4 h, but both the 25 K and 10 K stages took significantly longer because of their low cooling capacities and large thermal mass loads associated with the compliance tanks and JT components. Once the PT reached its bottom temperature, the JT stage would cool rapidly to its base temperature, within a few minutes if 0.2 MPa high-side pressure was used.

TOTAL POWER PROJECTION

Test data described above show that the design point cooling powers for the pulse tube require a nominal 150 W of compressor power. We have tested a variety of commercial off-the-shelf power electronic modules for driving the compressor and they generally had conversion efficiencies of better than 90 % power so the pulse tube will require a total power draw of about 165 W. Although the JT compressor is still under development, preliminary tests indicate that the power draw by the compressor and drive electronics will be about 50 W. If the power for cooling fans and thermometry/diagnostic instrumentation is included, the final total power draw may be well less than 250 W. We also evaluated power consumption if we used a smaller, commercially available, pulse tube compressor to reduce system weight, with the result that another 30 W of compressor power will be required.

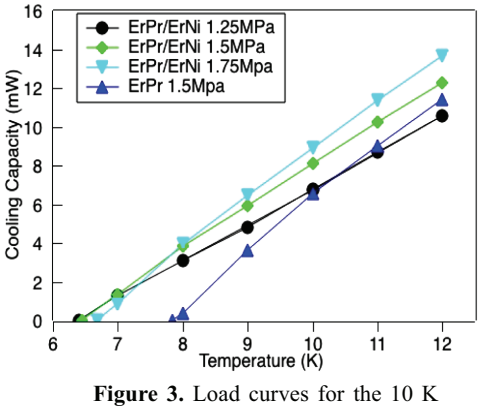

Figure 3. Load curves for the 10 K stage comparing the all ErPr regenerator to the ErPr/ErNi regenerator at pressures of 1.25 MPa, 1.5 MPa, and 1.75 MPa.

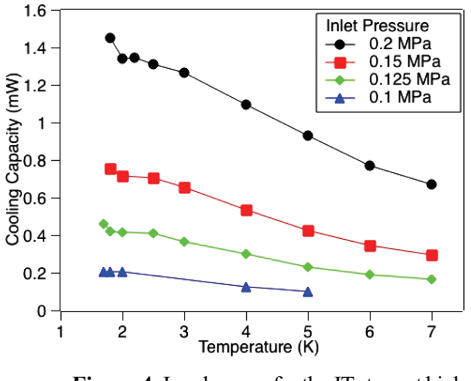

Figure 4. Load curves for the JT stage at high side pressures of 0.1 MPa, 0.125 MPa, 0.15 MPa, and 2 MPa.

EXPANDABILITY

These test results are for one operating condition for the pulse tube and one flow impedance for the JT stage. For low heat load applications, the flow impedance can be increased, reducing the mass flow, which would both reduce the power required for both the JT compressor and pulse tube compressor. Conversely, there is substantial upside in the cooling power capability of the JT stage. The JT impedance can be reduced, which would result in higher mass flow rates and higher cooling powers. The pulse tube has sufficient capacity to accommodate higher JT mass flow rates, so capacities approaching 5mW are possible, although this will require development of a larger capacity JT compressor.

Lower temperatures using ^{4}He are possible but will require a combination of reworking the JT counterflow heat exchanges to reduce pressure drop, a JT compressor with lower suction pressure, and superfluid film creep mitigation. Direct substitution with ^{3}He should result in temperatures below 1 K.

CONCLUSION

We have demonstrated a compact, low power pulse tube/JT hybrid cooler that reaches a base temperature of 1.7 K with up to 1.4 mW of cooling. We project that an SNSPD system using this cooler will have a total power draw of about 250 W and the entire unit will be rack mountable in a standard equipment rack. The component with the highest risk to reliable operation, the JT compressor, is presently under development.

ACKNOWLEDGMENT

This work was supported by the Laboratory of Telecommunications Sciences agreement No. EAO222214 and by the National Institute of Standards and Technology's Physical Measurement Laboratory to advance the goal of "Invisible Cryogenics."

REFERENCES

1. J. Hubmayr, J.E. Austermann, J.A. Beall, D.T. Becker, B. Dober, S.M. Duff, J. Gao, G.C. Hilton, C.M. McKenney, J.N. Ullom, J. Van Lanen, M.R. Vissers, "Low Temperature Detectors for CMB Imaging Arrays," *J. Low Temp. Phys*, to be published.
2. Ullom J.N. and Bennett, D. A., "Review of Superconducting Transition Edge Sensors for X-Ray and Gamma-Ray Spectroscopy," *Superconductor Science and Technology*, vol. 28, 084003 (2015).
3. Hadfield, R.H., "Single-Photon Detectors for Optical Quantum Information Applications," *Nature Photonics,* vol. 3 (2009), pp 696-705.
4. Kotsubo, V., et. al. "Compact 2.2K Cooling System for Superconducting Nanowire Single Photon Detectors," *IEEE Trans. Appl. Superconductivity,* vol. 27, Issue 4 (2017), pp 1-5.
5. F. Marsili, V.B. Verma, J.A. Stern, S. Harrington, A.E. Lita, T. Gerrits, I. Vayshenkar, B. Baek, M.D. Shaw, R.P. Mirin, and S.W. Nam, "Detecting Single Infrared Photons with 93% System Efficiency," *Nature Photonics* 7 (2013), pp 210-214.
6. B. Wang, L.Y. Wang, J.K. Zhu, J. Chen, Z.P. Li, Z.H. Gan, L.M Qiu, "Study of Phase Shifting Mechanism of Inertance tube at Low Temperatures," *Cryocoolers 17,* ICC Press, Boulder, CO (2012), pp 169-177.
7. A. Kashani, B.P.M Helvensteijn, J.R. Maddocks, P. Kittel, J.R. Feller, K.A. Gschneidner, V.K. Pecharsky, A.O. Pecharsky, "New Regenerator Materials for use in Pulse Tube Coolers,"*Cryocoolers 12*, Kluwer Academic/Plenum Publishers, New York (2003), pp 475-480.
8. J. H. So, G.W. Swift, and S. Backhaus, "An Internal Streaming Instability in Regenerators," J. Acous. Soc. Am. 120 (2006), pp 1898-1909.

9. Sage, Gedeon Associates, Athens, OH. Certain commercial equipment and software, are identified to describe the subject adequately. Such identification does not imply recommendation or endorsement by the NIST, nor does it imply that the equipment identified is necessarily the best available for the purpose.

10. G. W. Swift, *Thermoacoustics*, Springer International Publishing, (2017).

11. W. M Kays and A. L. London, *Compact Heat Exchangers*, McGraw-Hill (1984), pp 19-29.